LAWRENCE
LIVERMORE
NATIONAL
LABORATORY

UCRL-CONF-214749

Simulation of Positronium: Toward More Realistic Models of Void Spaces in Materials

A.L.R. Bug, T.W. Cronin, P.A. Sterne, Z.S. Wolfson

August 22, 2005

8th International Workshop on Positron and Positronium Chemistry (PPC8)
Coimbra, Portugal
September 4, 2005 through September 9, 2005

Simulation of Positronium: Toward more realistic models of void spaces in materials

Amy L.R. Bug, [a,*] Timothy W. Cronin, [a] P.A. Sterne, [b] Zachary S. Wolfson [a]

[a] *Department of Physics and Astronomy, Swarthmore College, Swarthmore, PA, 19081, U.S.A*

[b] *Lawrence Livermore National Laboratory, P.O. Box 808, L-045, Livermore, CA 94550, U.S.A.*

Abstract

An exact treatment of the positron and electron in a two-chain, Path Integral Monte Carlo (PIMC) simulation is used to calculate both self-annihilation and pickoff rates at finite temperature. It has already been demonstrated that this technique can reproduce and extend results of simple theories of positrons and positronium (Ps) in spherical voids. Here, we include the effect of the linear dielectric response of a homogeneous material on the annihilation rate of positrons and Ps. In addition, we find lifetimes and structural information for Ps in cylindrical channels, both with and without adsorbed fluid atoms.

Key words: positron, positronium, void, simulation
PACS: 71.60+z, 78.70Bj

1 Introduction

Positron annihilation lifetime spectroscopy (PALS) of positronium (Ps) has been used extensively in gaining a knowledge of pore structure and contents in materials as diverse as minerals, polymers, glasses, and low-k dielectrics[1–5]. The extrapolation from lifetime to pore size in such materials is done almost exclusively using the Tao-Eldrup (TE) model or alternatively, a rectangular,

* Author to whom correspondence should be addressed

finite-temperature version, the RTE model [6,7]. In this paper, we will use the term "single-particle-in-a-box" (SPIB) to denote models like these, involving a single particle in a pore with hard walls and no dielectric response. We will reserve the label"TE" for a SPIB in the restricted case that (i) the pore is spherical (ii) the calculation is done for the ground state.

In this paper, we address three aspects of materials that go beyond these SPIB models. First, we consider the effects of dielectric response on a more realistic two-particle model of Ps[8]. We find that dielectric effects create better agreement with TE than one would otherwise expect. Second, we demonstrate a scaling relation between the radius of a cylinder and of a sphere in the TE approximation. Third, we explicitly model Ps and fluid particles in a pore. We confirm that the Ps creates a bubble at higher fluid densities and we find the pickoff rate with both the fluid and pore wall.

2 Methods and Models

2.1 Theory and general method

We model the annihilation rate Γ (inverse lifetime) in fluid-filled pores as the self-annihilation rate $\kappa\Gamma_0$ and pick-off annihilation rates from fluid and pore walls, $\Gamma_{\text{p.o.wall}}$ and $\Gamma_{\text{p.o.fluid}}$, operating in parallel [9]. Thus,

$$\tau^{-1} \equiv \Gamma = \kappa\Gamma_0 + \Gamma_{\text{p.o.wall}} + \Gamma_{\text{p.o.fluid}} \tag{1}$$

The self-annihilation rate for ortho-Ps in vacuum is Γ_0, κ is the internal contact density, and

$$\Gamma_{\text{p.o.wall}} = (2ns^{-1}) \int_{r=R_c-\Delta}^{r=R_c} n_+(\mathbf{r}) d^3r, \tag{2}$$

with $n_+(\mathbf{r})$ the positron density at location $\mathbf{r}$ in a pore of radius R_c, and Δ a shell thickness in which electronic density is assumed to be nonzero. In the current paper, we consider both vacant and fluid-filled pores. In the former case, $\Gamma_{\text{p.o.fluid}} = 0$. In the latter,

$$\Gamma_{\text{p.o.fluid}} = \pi r_e^2 c \int n_-(\mathbf{r}) n_+(\mathbf{r}) \gamma[n_-(\mathbf{r})] d^3r \quad . \tag{3}$$

The electronic density from the fluid, $n_-(\mathbf{r})$, can be found by superposing atomic charge densities given by a local Density Functional Theory (LDA-

DFT)[10]. Here, the enhancement factor [11] γ will be set to unity (the "independent particle model").

In order to calculate the positronic density, n_+, and internal contact density, κ, in Eqs. 1, 2 and 3, we employ Path Integral Monte Carlo. PIMC is a method which allows one to calculate $< \delta(\mathbf{r}) >$, the probability that the positron will occupy the position $\mathbf{r}$. More generally, it allows one to calculate the thermal average of observables[12,13]. PIMC methods have been used by a number of groups to study particles like electrons and positrons in fluids and microporous solids [8,14,15] . In this type of calculation, the light particles (in our case, e^+ and e^-) may be represented as polymeric chains of entities known as "beads"[16]. The two chains of beads interact through the Coulomb interaction, which we treat using a numerical interpolation of the exact Coulombic propagator[17].

Our calculations also require terms in $\hat{\rho}$ of the form $exp(-\beta\hat{V})$ to describe the sum total potential energy operator, $\hat{V}$, acting on e^+ and e^- within the material. For the contribution from the pore walls, we use an effective potential, $log\hat{G}(\beta)$. $\hat{G}$ is a propagator which obeys the Bloch equation and enforces the correct, hard-wall, boundary condition. For both spherical (Section 3) and cylindrical (Sections 4 and 5) pore geometries, we use a form for $\hat{G}(\beta)$ which is an approximation to the exact propagator for a planar wall[18]. (The plane in question is the tangent to the enclosing surface at a point closest to a bead.) For calculations of Ps in the presence of argon, we use pair potentials. The e^+-Ar potential is a single-atom Hartree potential obtained from LDA-DFT. The e^--Ar potential is fit to scattering data[19]. Correlation from atomic polarization is not included. Both of these potentials are wholly repulsive.

2.2 Dielectric model

The region beyond a spherical pore wall is modeled as a uniform dielectric material with dielectric constant k_o, greater than the dielectric constant $k_i = 1$ within the pore. The electric potential inside the sphere can be obtained by solving Laplace's equation with the appropriate boundary conditions[21,22]. The potential in Gaussian units due to a point charge q_j at location $\mathbf{r}_j$ within the sphere is:

$$\phi(\mathbf{r}) = \frac{q_j}{|\mathbf{r} - \mathbf{r_j}|} + \phi_j(\mathbf{r}) \ ;$$

$$\phi_j(\mathbf{r}) = \frac{q_j}{R_c}\frac{k_i - k_o}{k_i}\sum_{n=0}^{\infty}\frac{n+1}{nk_i + (n+1)k_o}\left(\frac{r_j r}{R_c^2}\right)^n P_n(\cos\theta_j), \qquad (4)$$

where θ_j is the angle between $\mathbf{r}_j$ and $\mathbf{r}$. The total potential in the cavity due to two charges is found by superposition. The e^+ and e^-, beads interact at the same imaginary time slice only. The cavity polarization part of the potential energy for beads at $\mathbf{r}_1$ and $\mathbf{r}_2$ is:

$$V_{pol}(\mathbf{r}_1, \mathbf{r}_2) = \frac{1}{2} q_1(\phi_1(\mathbf{r}_1) + \phi_2(\mathbf{r}_1)) + \frac{1}{2} q_2(\phi_1(\mathbf{r}_2) + \phi_2(\mathbf{r}_2)) \tag{5}$$

with ϕ_j defined as in Eq. 4. Of the four terms in Eq. 5, two represent the"self-energy" of the charges due to their own induced polarization, while the other two are the "cross-energy".

For self-energy, we calculate the first m terms of Eq. 4 explicitly, then make the approximation that $n + 1 \approx n$ for $n > m$ and apply the geometric correction term $\sum_{n=m}^{\infty} b^n = \frac{b^{m+1}}{1-b}$ with $b = \frac{r_j r}{R_c^2}$. For $m = 25$, the error is negligible. We cut off the series in Legendre polynomials for the cross-energy at a sufficient number of terms to permit 2% accuracy within a distance of $a = 0.1\ au$ of the pore wall, but we employ no correction term. As expected, polarization energies diverge as $\frac{1}{R_c - r_i}$ as $r_i \to R_c$; this Coulombic singularity renders our path integral algorithm unstable. We eliminate the instability in a standard way by introducing a Yukawa screening potential [20] which multiplies V_{pol} of Eq. 5 by the factor $(1 - e^{-(\frac{R_c - r_i}{a})})$, with $a = 0.132\ au$.

2.3 Fluid model

We simulate the behavior of Ar in a cylindrical pore via classical Metropolis Monte Carlo methods. After introducing Ar atoms in a regular packing scheme, we move them randomly, accepting trial moves with a probability corresponding to the thermal density matrix $\exp(-\beta V_f)$, with V_f the configurational potential energy. We employ a Lennard-Jones potential $U_{\mathrm{LJ}}(r)$ to model interactions between two Ar atoms:

$$U_{\mathrm{LJ}}(r) = 4\epsilon[(\sigma/r)^{12} - (\sigma/r)^6] \tag{6}$$

We use $\epsilon = 119.8$ K, and $\sigma = 3.405\ \mathring{A}$. To simulate an infinite cylinder, we implement periodic boundary conditions in the axial direction with a repeat length of five times the radius. Potentials are cut off at either half the cylinder height or 2.5 σ, whichever is less. The fluid atoms are displaced every 20 moves of e^+, e^- beads. In simulations, we generally allow $\sim 10^3$ Monte Carlo steps per Ar atom for equilibration before data collection. We aim for a 50% acceptance fraction using adaptive step sizes.

3 Spherical pores in a dielectric material

The dielectric polarizability of material outside the void has the effect of attracting the positron to the internal surface. The effect is particularly dramatic if the pore encloses a single e^+, rather than Ps. The main part of Fig. 1 depicts $\tau_{p.o.wall} = 1/\Gamma_{p.o.wall}$ (Eq. 2) for a single e^+. When $k_o = 1.0$ (the TE case) this lifetime rises as the volume, or R_c^3. Lifetime also increases for $k_o = 3$ but does not scale as the volume. To find the limiting value of $\tau_{p.o.wall}$ as $R_c \rightarrow \infty$, we can solve the Schrodinger equation for a positron outside of a flat, dielectric surface. If temperature is kept arbitrarily low so the positron remains in its ground state, $\tau_{p.o.wall} \rightarrow 11.12\ ns$.

The inset to Fig. 1 shows Ps pickoff lifetime data for two values of cavity radius, $R_c = 10$ and 20. The lifetime of caged Ps exceeds that of a single e^+, as we would expect from previous studies[8,23]. Interestingly, $\tau_{p.o.wall}$ is similar for Ps in a $k_o = 3$ solid and for the TE model. For $R_c = 20\ au$, $\tau_{p.o.wall}$ is 21, 25 ns for $k_o = 1,\ 3$. While modeling Ps in a hard pore as a two-particle system raises the pickoff lifetime, including the dielectric polarizability of the solid lowers the lifetime. Modeling both of these features results in good accord with the TE result.

Fig. 2 shows the radial probability density in a pore for the e^+ of Ps. (Integration over the outermost $\Delta = 3.13\ au$ of these curves produces the $R_c = 20\ au$ data of Fig. 1.) One clearly sees that the polarizable solid draws e^+ density toward the wall, lowering the lifetime from the $k_o = 1$ value. There is a complicated relationship between the TE and the $k_o = 3$, two-particle results. At about 3 au into the pore, these curves cross. At smaller radii, the e^+ of Ps is closer to the pore wall than would be calculated from the TE model; at larger radii, the opposite is true.

Table I shows the effect of dielectric constant on the Ps pickoff lifetime for pores of two radii. For the small micropore with $R_c = 6\ au$, the lifetime varies little. For $R_c = 10\ au$ however, $\tau_{p.o.wall}$ is lowered by a factor of almost two as the dielectric constant is increased from $k_o = 1$ to 15. Increasing k_o beyond this range does not produce a large, additional change in the lifetime. This might be expected from the fact that the strength of the polarization potential from Eq. 4 scales only from 0 to 1, varying as $(k_o - 1)/(k_o + 1)$.

The internal contact density, κ, is recognized to exceed unity in small model voids with hard walls[24,25]; this is one of the unphysical consequences of using such models. Setting $k_o > 1$ reduces κ, but in small micropores the increase in κ due to compression overwhelms its reduction due to dielectric shielding. In larger pores such as $R_c = 20\ au$, for $k_o = 3$ we find $\kappa = 0.96(1)$, a modest reduction from $\kappa = 1.00(1)$ for $k_o = 1$.

4 Annihilation in cylindrical pores

4.1 Comparison of ground-state Spherical and Cylindrical SPIB

The TE model has been used for many pores that are surely not spherical. Here we offer a possible explanation for the success of the standard TE model when applied to a system where pores are elongated to the point of being modeled by cylinders. The TE formula for pickoff is given by Eq. 2 which can be readily evaluated for ground states in both spheres and cylinders[26]. The dotted line in Fig. 3 shows that if we rescale the spherical radius R_0 by a factor $\alpha_{\rm cs} \approx 1.195$, the lifetimes are nearly identical. Agreement becomes successively better as R_0 grows. The greatest error is around 6%, at $R_0 \approx 5\ au$. The error drops to zero at large R_0 ; it is less than 1.5% for $R_0 > 1\ nm$. The rescaling factor $\alpha_{\rm cs}$ can be shown analytically to be $(\pi/\chi)^{2/3}$, where, $\chi \approx 2.4048$ is the first node of the Bessel function $\mathrm{J_0(x)}$, by equating the lowest order terms in a series expansion of the spherical and cylindrical probability densities near the wall[27]. The fact that the TE model predicts virtually the same lifetime for a cylinder of radius R_0 and a sphere of radius $\alpha_{\rm cs}R_0$ may help explain the robust utility of the TE model.

4.2 Beyond SPIB

When PIMC is used to simulate Ps at an arbitrary temperature in a cylindrical pore, a number of features emerge. The lifetime in a cylindrical pore is longer than in a spherical pore of the same radius, in agreement with SPIB results [29,30], including Section 4.1 above. The two-particle model lifetime is also longer than that of a SPIB with $m = 2m_e$ in the same pore. (Comparing equal masses is important - mass determines the admixture of excited states at finite temperature[6,7,31].) Lifetime decreases with temperature as one would expect as excited states enhance density near the wall. Some of these features are illustrated in Table II: lifetime data as in Eq. 1 for a micro- and small mesopore. The lower temperature involves only the ground state; the higher temperature excites an admixture of up to seven (for $R_c = 25$) states contributing at a level of greater than 0.1%. (Similar calculations are done for a spherical pore in Reference [28].)

In narrow pores, one can see the results of the "squeezing" of the orbitals, resulting in $\kappa \geqslant 1$. The orbital is simultaneously compressed in the radial and, as Fig. 4 demonstrates, axial direction. This is perhaps counterintuitive. However, compression is asymmetrical and becomes more so as the pore narrows. The mass quadrupole moment, $Q =< 3z^2 - r^2 >$, is $Q = 2, 1$ or $0.5\ au$ when

the pore radius is $R_c = 4, 6$, or 8 au.

5 Annihilation in fluid-filled pores

Fig. 5 shows the pickoff rate, from Eqs. 2, 3 for Ps in an Ar-filled cylindrical pore of radius $R_c = 16$ au. At this temperature, $T = 632K$, Ps is expected to be in a ground state. Plausibly, $\Gamma_{p.o.fluid}$, rises linearly at low ρ^*. At higher densities, the rate levels off. The not-too-surprising conclusion that a Ps bubble forms at higher ρ^* is not only apparent from an analysis of bead coordinate data, but is also apparent from the interesting shape of $\Gamma_{p.o.wall}$. For very low densities, it rises slightly. One might think of Ps as being "expanded" by isolated Ar atoms that are intercalated into Ps density. At higher densities the bubble excludes Ar. Ps is partially shielded by surrounding fluid from contact with the wall, so $\Gamma_{p.o.wall}$ falls as $\Gamma_{p.o.fluid}$ continues to rise. It would be interesting to examine the case of a very narrow pore, where the Ps "bubble" might fill the pore cross section, and show rather different behavior.

Acknowledgements

We thank A. de Lima, Z. Kajcsos, and the organizing committee of PPC-8 (Coimbra, 2005); and the Provost's Office, HHMI, Sigma Xi and Department of Physics and Astronomy of Swarthmore College. This work was performed under the auspices of the U.S. Department of Energy by University of California Lawrence Livermore National Laboratory under contract W-7405-Eng-48.

References

[1] Peng, J., Frieze, W.E., Vallery, R.S., Gidley, D.W., Moore, D.L. and Carter R.J., 2005. Revealing hidden pore structure in nanoporous thin films using positronium annihilation lifetime spectroscopy. Appl. Phys. Lett. 86, 121904-121907.

[2] Yang, S., Mirau, P., Sun, J., and Gidley, D.W., 2003. Characterization of nanoporous ultra low-k thin films templated by copolymers with different architectures. Rad. Phys. and Chem. 68 , 351-356.

[3] Faupel, F., Kanzow, J., Gunther-Schade, K., Nagel, C., Sperr, P., Kogel, G., 2004. Positron Annihilation Spectroscopy in Polymers. Mat. Sci. Forum 445-445, 219-223.

[4] Kajcsos, Zj., Guplatre, G., Liszkay, L., Lazar, K., Lohonyai, L., Pal-Borbely, G., Beyer, H.K., Caullet, P., Patarin, J. , 2001. Positrons and Positronium in Zeolites. Mat. Sci. Forum 363-365, 238-243.

[5] Jones, D.G., Fretwell, H.M., 2003. Condensation and Freezing of a Binary Gas Mixture Adsorbed in Mesoporous Vycor Glass. Langmuir 19, 9018-9022.

[6] Gidley, D.W., Frieze, W.E., Dull, T.L., Sun, J., Yee, A.F., Nguyen, C.V., and Yoon, D.Y., 2000. Determination of pore-size distribution in low-dielectric thin films. Appl. Phys. Lett. 76 , 1282-1284..

[7] Dull, T.L., Frieze, W.E., Gidley, D.W., Sun, J.N., Yee, A.F, 2001. Determination of pore size in mesoporous thin films from the annihilation lifetime of positronium. J. Phys. Chem. B 105, 4657-4662.

[8] Larrimore,, L., McFarland, R.N., Sterne, P.A., Bug, A.L.R., 2000. A Two-Chain Path Integral Model of Positronium. J. Chem. Phys. 113, 10642-10650.

[9] Dupasquier, A., 1983. Quasipositronium in Liquids and Solids. In: Brandt, W., Dupasquier, A., (Eds.) Positron Solid-State Physics, North Holland, New York, pp. 485-505.

[10] Sterne, P.A., Asoka-Kumar, P., Howell, R.H., 2002. Atomic-based calculations of two-detector Doppler-broadening Spectra. Appl. Surf. Sci. 194, 71-75.

[11] Puska, M.J., Nieminen, R.M, 1994. Theory of Positrons in Solids and on Solid Surfaces. Rev. Mod. Phys. 66 , 841-897.

[12] Ceperley, D.M., 1995. Path integrals in the theory of condensed helium. Rev. Mod. Phys. 67 , 279-355.

[13] Landau, D.P., Binder, K., 2000. A Guide to Monte Carlo Simulations in Statistical Physics, Cambridge Univ. Press, Cambridge, Ch. 8.2.

[14] Miller, B.N., Reese,T.L., 2002. Path integral simulation of positronium. Nucl. Inst. and Meth. in Phys. Res. B 192 , 176-179.

[15] Schmitz, H., Muller-Plathe, F., 2000. Calculation of the lifetime of positronium in polymers via molecular dynamics simulations. J. Chem. Phys. 112 , 1040-1045.

[16] Chandler, D., Wolynes, P.G., 1981. Exploiting the Isomorphism Between Quantum Theory and Classical Statistical Mechanics of Polyatomic Fluids. J. Chem. Phys. 74, 4078-4095.

[17] Pollock, E.L., 1988. Properties and computation of the Coulomb pair density matrix. Comput. Phys. Commun. 52 , 49-60.

[18] Whitlock, P.A., Kalos, M.H., 1979. Monte Carlo Calculation of the Radial Distribution Function of Quantum Hard Spheres at Finite Temperatures. J. Comp. Phys. 30 , 361-388.

[19] Space, B., Coker, D.F., Liu, Z.H., Berne, B.J., Martyna, G., 1992. Density dependence of excess electronic ground-state energies in simple atomic fluids. J. Chem. Phys. 97 , 2002-2021.

[20] Muser, M.H., Berne, B.J., 1997. Circumventing the pathological behavior of path-integral Monte Carlo for systems with Coulomb potentials. J. Chem. Phys. 107 , 571-575.

[21] Jackson, J.D.,1999. Classical Electrodynamics, 3rd ed. Wiley, New York, Ch. 4.

[22] Griffiths, D.J., 1999. Introduction to Electrodynamics. Prentice Hall, New Jersey, pp. 191-193.

[23] Sterne, P.A., Larrimore, L., Hastings, P., Bug, A.L.R., 2003. New Theories For Positrons in Insulators. Radiation Physics and Chemistry 68 , 409-414.

[24] Brandt, W., Berko, S., Walker, W.W., 1960. Positronium decay in molecular substances. Phys. Rev. 120 , 1289-1295.

[25] Dryzek, J., 1999. Calculations of Annihilation Rate of o-Ps in Pick-off Process. Acta Phys. Polon. 95 , 527-532.

[26] In spheres, the familiar TE result emerges: $\Gamma_{p.o.wall} = 2(1 - \frac{R_0-\Delta}{R_0} + \frac{1}{2\pi}\sin\frac{2\pi(R_0-\Delta)}{R_0})$. In cylinders, the result cannot be expressed in terms of elementary functions, but evaluation with *Mathematica*$^{\mathrm{TM}}$is straightforward.

[27] Cronin, T.W., and Bug, A.L.R., 2005. PIMC Simulation of Positronium: Cylindrical Pores and an Extension of the Standard Model. Poster presented at 8th International Workshop on Positrons and Positronium Chemistry, Coimbra, Portugal.

[28] Bug, A.L.R. and Sterne, P.A., 2005. PIMC simulation of Ps annihilation: From micro to mesopores. (preprint)

[29] Consolati, G., 2002. Positronium trapping in small voids: Influence of their shape on positron annihilation results. J. Chem. Phys. 117, 7279-7283.

[30] Jean, Y.C., Shi, H., 1994. Positronium lifetime in an ellipsoidal free-volume hole of polymers. J. Non-Crystalline Solids 172-174, 806-814.

[31] Goworek, T., Ciesielski, K., Jasinka, B., Wawryszczuk, J., 1997. Positronium in large voids. Silicagel. Chem. Phys. Lett . 272, 91-95.

k_o	$\tau_{p.o.wall}:\ R_c = 6au$	$\tau_{p.o.wall}:\ R_c = 10au$
1	1.10(5)	4.8(2)
2	1.06(1)	4.1(2)
3	1.03(1)	3.5(2)
5	1.005(10)	3.0(2)
15	0.99(1)	2.7(1)

Table I: Pickoff lifetime in ns as a function of k_o for Ps in spherical micropore. For both radii, Ps is in cavity ground state.

$R_c\ (au)$	$T\ (K)$	τ	τ_{SPIB}
8	6320	3.27(1)	2.29
8	1000	3.82(5)	2.57
25	1000	53(1)	38.7
25	300	72(10)	45.0

Table II: Lifetime (pickoff plus self-annihilation) in ns for Ps in cylindrical micro- and mesopores at temperature T. Pickoff occurs within $\Delta = 3.13\ au$ of wall. Lifetime τ from two-particle PIMC calculation. SPIB lifetime, τ_{SPIB} found by summing series of Bessel functions with appropriate thermal weights, assuming a single particle of mass $2m_e$ at temperature T.

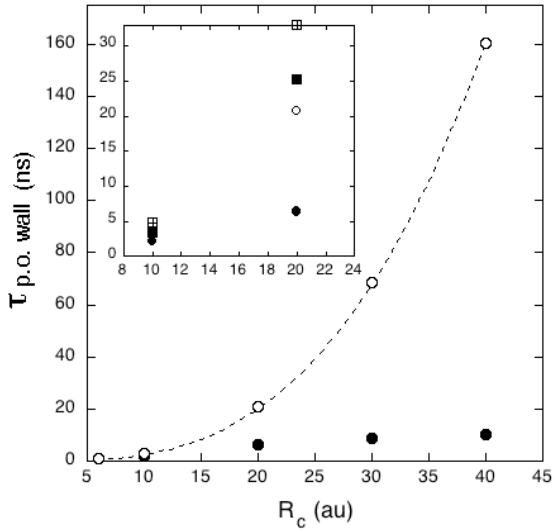

Fig. 1. Pickoff lifetime as a function of spherical pore radius, R_c. Main part of figure shows lifetime of e^+. Open circles: $k_o = 1$; filled circles: $ko = 3$. Inset of figure includes square symbols showing lifetime of Ps. Open square with plus-sign: $k_o = 1$; filled square: $k_o = 3$. All data for Ps in cavity ground state.

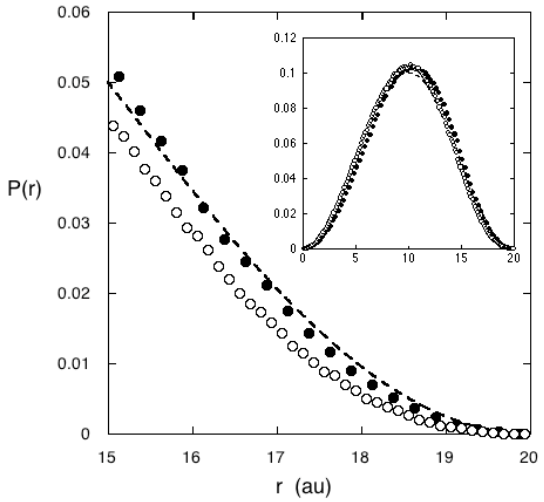

Fig. 2. The radial probability density for Ps in the ground state of a spherical pore of radius $R_c = 20\ au$. Open circles: $k_o = 1.0$; filled circles: $k_o = 3.0$; dashed line: TE result. The main figure provides a close-up view of density in the outer 5 au of the pore. The inset shows the density for all radii within the pore.

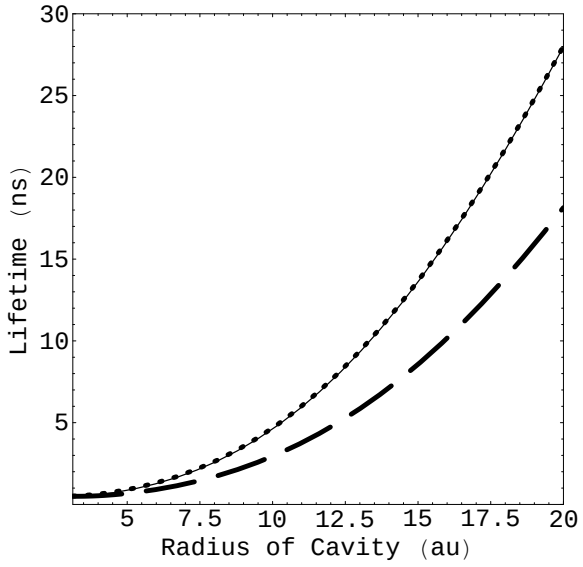

Fig. 3. SPIB lifetimes as a function of cavity radius, R_0. Thick dashed line is spherical (TE) geometry result; thin solid line is cylindrical geometry result; dotted line is spherical (TE) geometry result with cavity radius rescaled by factor $\alpha_{\rm cs}$.

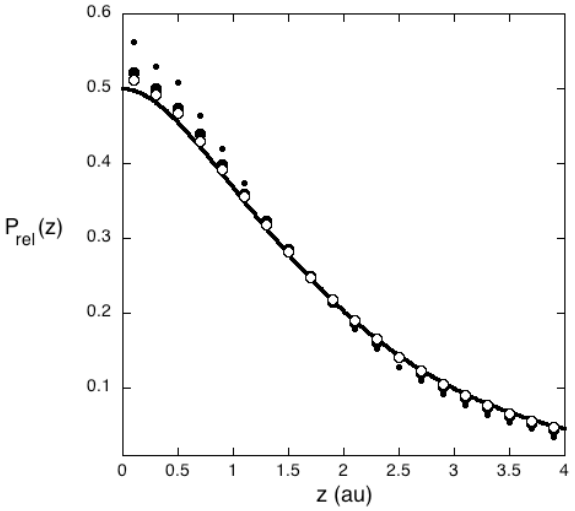

Fig. 4. Distribution function in z, the component of the Ps relative coordinate along the cylinder axis. Temperature $T = 1000K$ implies Ps is in ground state in cavity. Small filled circles: $R_c = 4\ au$; Large filled circles: $R_c = 6\ au$; Large open circles: $R_c = 8\ au$. Solid line: $R_c = \infty$ (free Ps) result. This is found by integrating the free Ps ground state density $|\Psi(r)|^2 = 1/8\pi\ exp(-r)$ where $r = \sqrt{\rho^2 + z^2}$ over ρ, to obtain $P_{rel}(z) = \frac{1}{2} exp(-|z|)(1 + |z|)$.

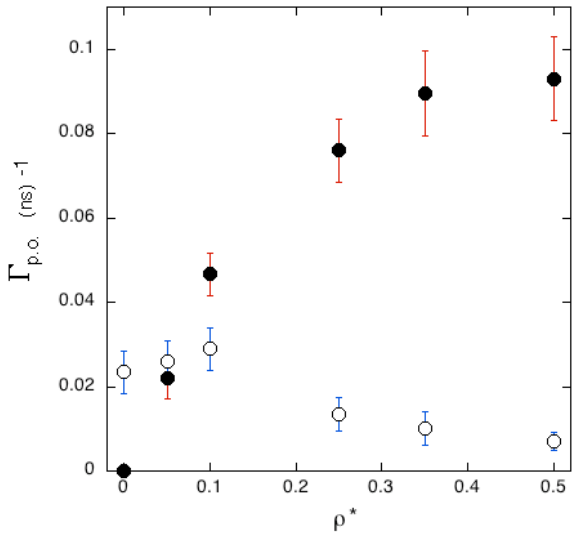

Fig. 5. The pickoff annihilation rate for Ps in a $R_c = 16\ au$ cylindrical pore taken at a temperature of $T = 632K$. Filled circles: pickoff rate with Ar atoms, $\Gamma_{p.o.fluid}$; Open circles: pickoff rate with the wall, $\Gamma_{p.o.wall}$.